

Nonlinear Dynamics and Deterministic Chaos

The aim of this chapter is to provide an introduction to the theory of nonlinear systems. We assume that the reader has a background in classical dynamics and a basic knowledge of differential equations, but most readers of this book will only have a vague notion of chaotic dynamics. The computer experiments in the following chapters will (hopefully) lead to a better understanding of this new and exciting field. These chapters form the core of the book and are written at a level suitable for advanced undergraduate students. An understanding and interpretation of the numerical results is, however, impossible without a knowledge of the relevant theory.

The theory of dynamical systems is well-developed and a number of excellent textbooks [1]–[8], as well as collections of important original articles [9]–[11], are available. The reader is invited to consult these references while exploring nonlinear dynamics on the computer. The overview of the theory of nonlinear dynamics presented in the following serves as a short survey, describing the basic phenomena and clarifying the notation used in the setup and analysis of the computer experiments.

The first three sections introduce *Deterministic Chaos* and the special cases of chaotic dynamics in *Hamiltonian Systems* and *Dissipative Dynamical Systems*. It is hoped that the reader will gain a basic understanding on going through these sections. Many features, however, will become clearer only later on in the context of the computational studies, which are linked to this introductory chapter by ample cross-references.

The last section of this chapter, *Special Topics*, contains additional material, which is useful for a more detailed understanding of certain aspects of chaotic dynamics introduced in the subsequent chapters. This section can (and should) be omitted in a first reading of the text.

2.1 Deterministic Chaos

‘*Deterministic chaos*’ is a term used to denote the irregular behavior of dynamical systems arising from a strictly deterministic time evolution without any source of noise or external stochasticity. This irregularity manifests itself in an extremely sensitive dependence on the initial conditions, which precludes any long-term prediction of the dynamics. Most surprisingly, it turned out that such chaotic behavior can already be found for systems with a very low degree of freedom and it is, moreover, *typical* for most systems.

A *dynamical system* can be described simply as a system of N first-order differential equations

$$\frac{dx_i}{dt} = f_i(x_1, \dots, x_N, r) \quad , \quad i = 1, \dots, N, \quad (2.1)$$

where the independent variable t can be read as time and the $x_i(t)$ are dynamical quantities whose time dependence is generated by (2.1), starting from specified initial conditions $x_i(0)$, $i = 1, \dots, N$. It should be noted that the system (2.1) is autonomous because it is not explicitly t -dependent. The f_i are nonlinear functions of the x_i and are characterized by the parameter(s) r . The equations lead to chaotic motion, which develops and changes its characteristics with varying control parameter(s) r . The assumption of an autonomous system is not essential, because otherwise it can be converted into an autonomous one by introducing the time t as an additional variable x_{N+1} . Examples of dynamical systems are the Hamiltonian equations of motion in classical mechanics, the rate equations for chemical reactions or the evolution equations in population dynamics.

A *discrete dynamical system* is an iterated mapping

$$x_i(n+1) = f_i(x_1(n), \dots, x_N(n), r) \quad , \quad i = 1, \dots, N \quad (2.2)$$

starting from an initial point $x_i(0)$, $i = 1, \dots, N$. Such a discrete system may appear quite naturally from the setup of the problem under consideration, or it may be a reduction of the continuous system (2.1) in order to simplify the analysis, as for example the Poincaré map described below.

Basically, one can make a distinction between *conservative* (e.g., mechanical systems governed by Hamilton’s equations of motion) and *dissipative* systems with ‘friction’. In the first case, volume elements in phase space are conserved, whereas dissipative systems contract phase space elements. This results in markedly different behavior.

2.2 Hamiltonian Systems

In a so-called Hamiltonian system with N degrees of freedom, the dynamics is derived from a Hamiltonian $H(\mathbf{p}, \mathbf{q}, t)$, where $\mathbf{q} = (q_1, \dots, q_N)$ and $\mathbf{p} = (p_1, \dots, p_N)$ are the canonical coordinates and momenta. The Hamiltonian equations of motion

$$\dot{p}_i = -\frac{\partial H}{\partial q_i}, \quad \dot{q}_i = \frac{\partial H}{\partial p_i}, \quad i = 1, \dots, N \quad (2.3)$$

generate trajectories $\mathbf{p}(t)$, $\mathbf{q}(t)$ in $2N$ -dimensional phase space. In more global terms, it is said that the Hamiltonian produces a flow in phase space. This flow conserves the phase space volume

$$dp_1 \dots dp_N dq_1 \dots dq_N \quad (2.4)$$

as well as the phase space ‘area’

$$d\mathbf{p} \cdot d\mathbf{q} = \sum_i dp_i dq_i. \quad (2.5)$$

2.2.1 Integrable and Ergodic Systems

In many cases, the Hamiltonian does not depend explicitly on time and the energy $E = H(\mathbf{p}, \mathbf{q})$ is conserved along the trajectory, i.e., it is a constant of motion. A simple example of such a conservative system is the motion of a particle with mass m in a potential V with Hamiltonian

$$H(\mathbf{p}, \mathbf{q}) = \frac{\mathbf{p}^2}{2m} + V(\mathbf{q}). \quad (2.6)$$

There may be more constants of motion, which can be a consequence of obvious symmetries of the system. Well-known examples are translational symmetry leading to conservation of the momentum or rotational symmetry resulting in angular momentum conservation. In other cases, the (possibly existing) constants of motion are far less obvious and it is a non-trivial problem to find them or to prove their existence. It is, however, simple to show that a given phase space function $F(\mathbf{p}, \mathbf{q})$ is a constant of motion. This can be most elegantly done by writing the equation of motion for F in terms of the Poisson bracket

$$\{A, B\} = \sum_i \left(\frac{\partial A}{\partial p_i} \frac{\partial B}{\partial q_i} - \frac{\partial B}{\partial p_i} \frac{\partial A}{\partial q_i} \right) \quad (2.7)$$

between two arbitrary phase space functions $A(\mathbf{p}, \mathbf{q})$ and $B(\mathbf{p}, \mathbf{q})$ as

$$\frac{dF}{dt} = \{H, F\} \quad (2.8)$$

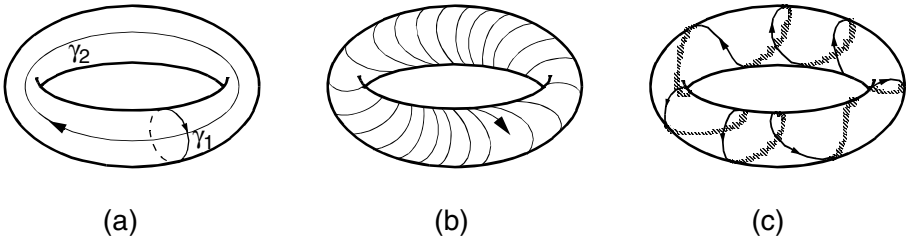


Fig. 2.1. Two-dimensional torus in phase space: (a) Topologically different paths γ_i . (b) A typical quasiperiodic trajectory. (c) Torus supporting periodic orbits.

(a simple example of these generalized equations comprises the canonical equations of motion (2.3)). Therefore, F is a constant of motion if the Poisson bracket with H vanishes identically

$$\{H, F\} \equiv 0, \quad (2.9)$$

which can easily be checked for a given F .

The existence of a constant of motion severely restricts the dynamical possibilities of a trajectory $(\mathbf{p}(t), \mathbf{q}(t))$, because it must follow the (hyper)surface $F(\mathbf{p}(t), \mathbf{q}(t)) = \text{constant}$. The motion is even more restricted if additional constants of motion exist. In the extreme case, the dynamical equations can be integrated in closed form. A system is said to be ‘*integrable*’ if N independent constants of motion F_j exist:

$$F_j(\mathbf{p}, \mathbf{q}) = c_j = \text{constant}, \quad j = 1, \dots, N. \quad (2.10)$$

One of the F_j can be the energy. In addition, the F_j must be ‘in involution’, i.e., their pairwise Poisson brackets must vanish:

$$\{F_j, F_k\} = \sum_i \left(\frac{\partial F_j}{\partial p_i} \frac{\partial F_k}{\partial q_i} - \frac{\partial F_k}{\partial p_i} \frac{\partial F_j}{\partial q_i} \right) = 0. \quad (2.11)$$

In this case, it can be shown that the phase space trajectory is confined to the surface of an N -dimensional manifold in $2N$ -dimensional phase space. Furthermore, it can be shown that this surface has the topology of a torus. The whole phase space is filled with such tori and the phase space flow is therefore highly organized and regular.

For systems with two degrees of freedom as, for example, the motion of a mass m in a two-dimensional potential $V(x, y)$ with Hamiltonian

$$H(p_x, p_y, x, y) = \frac{1}{2m} (p_x^2 + p_y^2) + V(x, y), \quad (2.12)$$

the solution of the equations of motion

$$\dot{p}_x = -\frac{\partial V}{\partial x} \quad , \quad \dot{x} = \frac{p_x}{m} \quad (2.13)$$

$$\dot{p}_y = -\frac{\partial V}{\partial y} \quad , \quad \dot{y} = \frac{p_y}{m} \quad (2.14)$$

describes the time evolution of the system in four-dimensional phase space (x, y, p_x, p_y) . Because of energy conservation, the trajectory is restricted to the three-dimensional manifold $H(p_x, p_y, x, y) = E$, the ‘energy surface’. For an integrable system, because of (2.11), there exists a second integral of motion with vanishing Poisson bracket with the Hamiltonian H . To take a specific example, we can assume that the potential is rotationally symmetric, $V(x, y) = V(x^2 + y^2)$, with constant angular momentum $L = xp_y - yp_x$.

This restricts the trajectory to a two-dimensional submanifold of the energy surface, which has the topology of a torus, as illustrated in Fig. 2.1. Such a torus is invariant under the equations of motion and is, therefore, referred to as an ‘*invariant torus*’. It should be stressed, however, that a two-dimensional torus embedded in four-dimensional phase space can be bent and twisted in a complicated manner, and that Fig. 2.1 is only a schematic illustration.

The torus topology can now be utilized in a theoretical analysis to introduce new canonical coordinates and momenta, namely the so-called ‘action-angle variables’ with actions $\mathbf{I} = (I_1, I_2)$ and angles $\boldsymbol{\varphi} = (\varphi_1, \varphi_2)$, allowing a solution — an integration — of the equation of motion in closed form. The actions are given by the phase integrals

$$I_i = \frac{1}{2\pi} \oint_{\gamma_i} \mathbf{p} d\mathbf{q} \quad , \quad i = 1, 2 \quad , \quad (2.15)$$

where γ_1 and γ_2 are two topologically different closed paths on the torus (see Fig. 2.1(a)), as discussed in any textbook of analytical mechanics. Written in action-angle variables, the Hamiltonian is simply given by $H = H(I_1, I_2)$ and — introducing the frequencies $\omega_i = \partial H / \partial I_i$, $i = 1, 2$ — the equations of motion simplify to

$$\dot{\mathbf{I}} = 0 \quad , \quad \dot{\boldsymbol{\varphi}} = \boldsymbol{\omega} \quad , \quad (2.16)$$

with the solution

$$\mathbf{I} = \text{constant} \quad \boldsymbol{\varphi}(t) = \boldsymbol{\varphi}(0) + \boldsymbol{\omega} t \quad . \quad (2.17)$$

The trajectory is quasiperiodic, characterized by the two frequencies ω_1 and ω_2 , and, typically, it covers the entire torus in the long-time limit. For the case of commensurable frequencies, i.e., frequencies whose ratio is rational, the trajectory returns precisely to its starting point and the identical orbit is traced out again: the trajectory is periodic (Fig. 2.1(c)). Moreover, the rationality condition is valid for the entire torus and all trajectories on this torus are periodic with the same period. The frequencies vary, of course, in phase space and therefore, typically, a dense, countable subset of the tori filling the

phase space carry periodic trajectories. This picture can easily be extended to the case of more than two degrees of freedom.

Integrable systems are rare. Until recently, however, such systems were almost exclusively treated in textbooks on classical dynamics, as for instance a forced or parametrically excited harmonic oscillator, a point mass in a three-dimensional spherically symmetric potential, N -dimensional coupled harmonic oscillators, etc. This led to the impression that the well-organized behavior of integrable cases is typical for systems with few degrees of freedom.

As another extreme example we have *ergodic* systems. Here, almost every trajectory approaches arbitrarily close to every energetically allowed point in phase space, i.e., it fills the phase space. Ergodic systems have been discussed in physics mainly in the context of a statistical description of systems with many degrees of freedom, e.g., the N -particle gas in thermodynamics ($N \sim 10^{23}$). Only in the last decades has it been realized that low dimensional physical systems can be ergodic.

Ergodicity, however, does not guarantee the decay of correlations in the long time limit, which is demanded for the so-called *mixing systems*. These systems lose the memory of their history and show irregular (or ‘chaotic’) behavior. A characteristic of such chaotic dynamics is an extreme sensitivity to initial conditions (exponential separation of neighboring trajectories), which puts severe limitations on any forecast of the future fate of a particular trajectory. This sensitivity is known as the ‘butterfly effect’: the state of the system at time t can be entirely different even if the initial conditions are only slightly changed, i.e., by a butterfly flapping its wings.

A quantitative measure of this exponential growth of deviations is given by the *Lyapunov exponent* (see Sect. 2.4.3). The most chaotic systems are the so-called *K-systems*. These are systems where nearby orbits separate exponentially. Very few systems have been proven to be mixing, as are, for example, the hard-sphere gas and the stadium billiard (see Chap. 3). A typical system (for two and more degrees of freedom) shows an intricate mixture of regular and irregular motion.

2.2.2 Poincaré Sections

In order to analyze complicated dynamics, one introduces a surface of section in phase space and, instead of studying a complete trajectory, one monitors only the points of its intersection with this surface. In this manner, we obtain a discrete mapping — the *Poincaré map* — which maps an intersection point onto the next one. As an illustrative example we again consider the Hamiltonian (2.12) with two degrees of freedom and take a section through phase space at, e.g., $y = 0$ for a given value of the energy E . Any point on this surface of section with coordinates (x, p_x) uniquely determines an initial point for a trajectory. Solving for p_y yields $p_y = \pm \{2m(E - p_x^2 - V(x, 0))\}^{1/2}$. The value of p_y is uniquely determined by the coordinates (x, p_x) in the Poincaré section if we fix the sign of p_y , following the convention of considering only

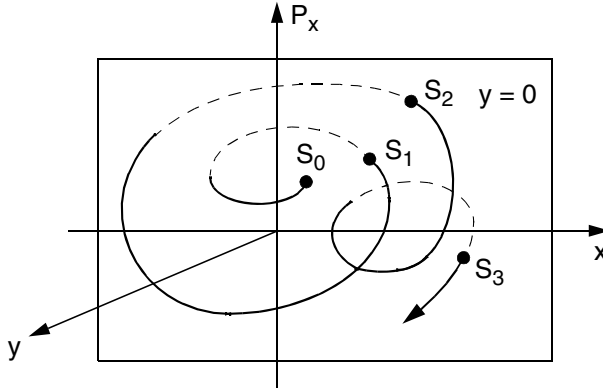


Fig. 2.2. A Poincaré section reduces the dynamics to a discrete mapping.

those trajectories which intersect the surface in the positive y -direction $p_y > 0$.

The dynamics then reduces to the discrete two-dimensional Poincaré mapping

$$S_n = (p_{x_n}, x_n) \xrightarrow{T} (p_{x_{n+1}}, x_{n+1}) = S_{n+1}, \quad (2.18)$$

as illustrated in Fig. 2.2. A simple proof shows that this map is area-preserving. The set of all such intersection points

$$T^n(p_{x_0}, x_0) = \underbrace{T \circ T \circ \cdots \circ T}_{n \text{ -times}}(p_{x_0}, x_0) \quad (2.19)$$

allows a much better insight into the dynamical behavior of the orbit as, for example, the trajectory in coordinate space, and a synoptic picture of different orbits quite easily provides an overview of the global properties of the phase space flow.

Orbits with

$$T^k(p_{x_0}, x_0) = (p_{x_0}, x_0) \quad (2.20)$$

are called k -periodic. These fixed points of the mapping T^k and their stability properties (see Sects. 2.4.4 and 2.4.5) can play an important role in the organization of the phase space flow and the Poincaré map. It should be noted that k -periodic orbits appear as a set of k discrete points in such a map. A quasiperiodic trajectory fills a closed curve in the Poincaré section, which is the intersection of the invariant torus covered by the trajectory and the Poincaré section. For an integrable system at fixed energy E , the surface of section is filled with a family of such ‘invariant curves’, i.e., curves invariant under the Poincaré map (2.18), as shown in Fig. 2.3. A countable subset of these invariant curves is filled with orbits, which are periodic under the Poincaré map.

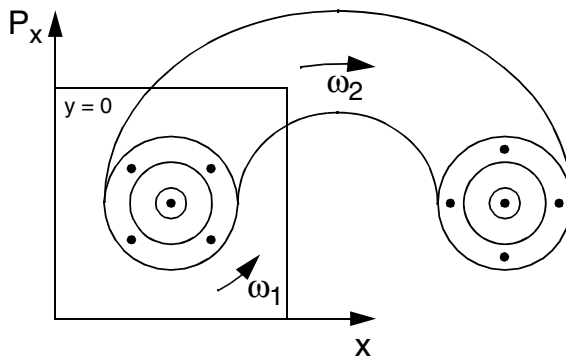


Fig. 2.3. A family of invariant tori in phase space appears as invariant curves in a Poincaré section. A subset of these invariant curves is filled with periodic orbits.

Poincaré sections and mappings are used in most of the computer programs described in the following chapters. In some cases, they arise directly from the physics of the dynamical system, as for example the mapping between subsequent impacts in billiard systems (Chap. 3 and 4). Another kind of Poincaré mapping appears for time-periodically driven systems (period T), where the state of the system is only observed at discrete times $t_n = nT$, generating a so-called stroboscopic mapping. Such a mapping is used in the studies of the Duffing oscillator (Chap. 8) and the Chaos generator (Chap. 10).

2.2.3 The KAM Theorem

For an integrable system, the entire phase space is filled with invariant tori and any trajectory will remain on the particular torus selected by the initial conditions. The proof of the existence of these tori is, however, based on the integrability of the system, i.e., the existence of N integrals of motion. It is now of considerable interest to investigate the behavior of the system when the integrals of motion are destroyed. This can be achieved by a small perturbation. To take an example, in a two-dimensional potential with rotational symmetry, the symmetry can be disturbed by a superimposed field and the angular momentum is no longer conserved. In this case, there is a priori no confinement to a two-dimensional submanifold of phase space, and the trajectory may explore all those parts of the phase space which are energetically accessible. This is, however, not the case.

The transition from an integrable to a nonintegrable system is most clearly analyzed in one of the most fundamental results in the theory of Hamiltonian (conservative) systems: the celebrated theorem of Kolmogoroff, Arnold, and Moser, which describes the influence of perturbations on an integrable system. Here, we formulate this so-called ‘*KAM theorem*’ for two degrees of freedom.

The KAM theorem assumes a perturbation of an integrable system H_0 by a term H_1 :

$$H(\mathbf{p}, \mathbf{q}) = H_0(\mathbf{p}, \mathbf{q}) + \varepsilon H_1(\mathbf{p}, \mathbf{q}) \quad (2.21)$$

(the mathematical proof requires certain differentiability properties of H_1). The parameter ε measures the strength of the perturbation. The essence of the KAM theorem is the surprising result that most of the invariant tori survive, i.e., the tori still exist in the perturbed system, although slightly deformed, and the trajectory still covers a two-dimensional subset of the phase space. The stability of an invariant torus against perturbation depends on the degree of non-periodicity of the motion on the torus, i.e., the irrationality of the ratio of the two frequencies ω_1 and ω_2 (we will assume that ω_1 is the smaller of the frequencies).

Formulated more precisely, all invariant tori with

$$\left| \frac{\omega_1}{\omega_2} - \frac{r}{s} \right| > \frac{K(\varepsilon)}{s^{5/2}} \quad (2.22)$$

for arbitrary coprime integer numbers r and s are preserved in the perturbed system. The constant $K(\varepsilon)$ depends only upon the perturbation strength ε , and goes to zero for $\varepsilon \rightarrow 0$.

Excluded from the stability criterion (2.22) are, in particular, tori with rational frequency ratio carrying periodic trajectories. Moreover, around each rational frequency ratio $\omega_1/\omega_2 = r/s$ there exists a narrow region of width $K(\varepsilon)s^{-5/2}$, in which (2.22) is not satisfied. For increasing ‘irrationality’ of the frequency ratio, i.e., larger denominator s in r/s , the region (2.22) guaranteeing preservation of the invariant tori decreases. Since the set of rational values of ω_1/ω_2 in the interval $[0, 1]$ is dense and for every rational frequency ratio r/s an entire interval

$$\left| \frac{\omega_1}{\omega_2} - \frac{r}{s} \right| \leq \frac{K(\varepsilon)}{s^{5/2}} \quad (2.23)$$

is excluded, one may conclude that (2.22) is practically never satisfied. This is, however, not the case. Figure 2.4 illustrates the destroyed zones for the most important r/s resonances, i.e., those with a small denominator ($s = 2, \dots, 7$). Here, the value of the constant $K(\varepsilon)$ is chosen as 0.3. One observes that the width of the destroyed zones decreases rapidly with increasing s . But, nevertheless, there are infinitely many of them.

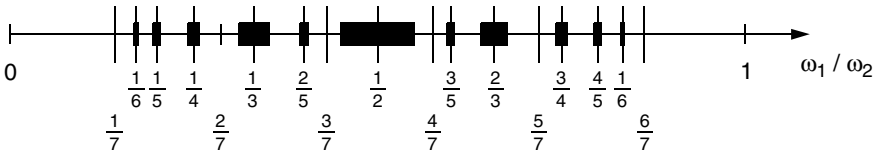


Fig. 2.4. Destroyed zones of length $K/s^{2.5}$ at rational frequency ratio r/s .

A simple estimate yields for the union of all these intervals (2.23)

$$\begin{aligned} \sum_{r < s} \left| \frac{\omega_1}{\omega_2} - \frac{r}{s} \right| &\leq \sum_s \sum_{r < s} K(\varepsilon) s^{-5/2} \\ &\leq \sum_s s K(\varepsilon) s^{-5/2} = K(\varepsilon) \sum_s s^{-3/2}. \end{aligned} \quad (2.24)$$

The last sum converges and, therefore, the sum over all intervals (2.23) goes to zero for $\varepsilon \rightarrow 0$, so that for a sufficiently weak perturbation the phase space volume not filled with invariant curves can be made arbitrarily small.

The invariant tori in the zones excluded by the KAM condition are in most cases destroyed. In the centers of the destroyed zone we have a torus with rational frequency ratio and, hence, periodic motion. In a simplified picture, one can imagine that, for such a periodic motion, the perturbation is also felt periodically, so that initially small changes induced in the trajectories may in time blow up, giving rise to large scale deviations. In addition to the rational torus, an interval given approximately by (2.23) is also destroyed.

The characteristic scenario for the subsequent destruction of invariant tori with increasing perturbation strength is discussed in more detail in Sect. 2.4.1. Here, we only note that a torus filled with periodic orbits with frequency ratio $\omega_1/\omega_2 = r/s$ quite typically decays. A number of νs stable and νs ($\nu \in \mathbb{N}$) unstable periodic orbits are, however, still existent, where the integer ν is often equal to one (a periodic trajectory is called ‘*stable*’ if nearby trajectories remain close to it for all times).

In a Poincaré section, these s -periodic trajectories which persist in the perturbed system appear as stable or unstable fixed points of the iterated Poincaré map T^s . The stability properties of such fixed points are studied in Sect. 2.4.5, where the use of the terms ‘*elliptic*’ and ‘*hyperbolic*’ for stable and unstable fixed points, respectively, is explained. The stable fixed points appear as centers of elliptic stability islands, as shown schematically in Fig. 2.5. A magnification of the neighborhood of such a fixed point appears to be almost self-similar to the original Poincaré section. The fixed point is surrounded by invariant curves, and between these invariant curves we find destroyed zones with alternating elliptic and hyperbolic fixed points. Magnifying the elliptic points again yields a similar picture. This process can be continued down to arbitrarily small scales (see Sect. 2.4.1 for more details).

2.2.4 Homoclinic Points

The neighborhood of the hyperbolic (i.e., unstable) fixed points looks very different and it is in this region that chaotic dynamics first develops. We define the ‘*stable manifold*’ H^+ of the hyperbolic fixed point (p_h, x_h) as the set of points in the Poincaré section approaching the hyperbolic fixed point after infinitely many iterations:

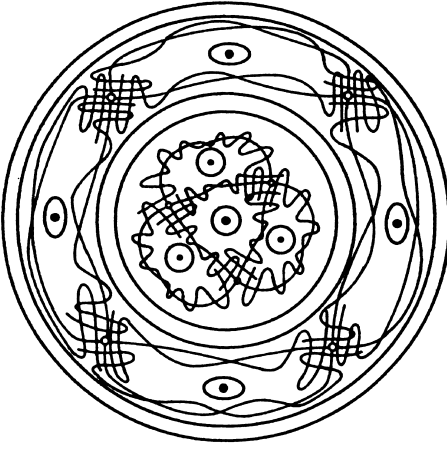


Fig. 2.5. Intact invariant curves and destroyed zones with chains of alternating elliptic and hyperbolic fixed points.

$$H^+ = \{(p, x) \mid \lim_{n \rightarrow \infty} T^n(p, x) = (p_h, x_h)\}. \quad (2.25)$$

The ‘*unstable manifold*’ H^- is the set of all points emanating from the fixed point after an infinite number of iterations:

$$H^- = \{(p, x) \mid \lim_{n \rightarrow \infty} T^{-n}(p, x) = (p_h, x_h)\}. \quad (2.26)$$

This is illustrated in Fig. 2.6.

One can convince oneself that the stable manifold H^+ has no self-crossings, because of the continuity of the map. The same is true for H^- . There are, however, crossings of H^+ and H^- and, moreover, these crossings occur generically. Such crossing points are called ‘*homoclinic points*’ if the two manifolds belong to the same fixed point, or ‘*heteroclinic points*’ for a crossing of stable and unstable manifolds of different fixed points.

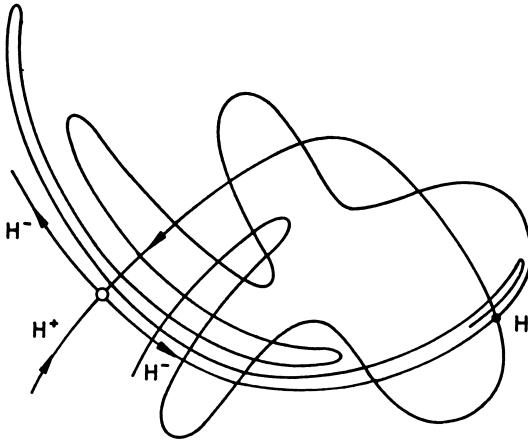


Fig. 2.6. The stable and unstable manifold H^+ and H^- of a hyperbolic fixed point (\circ) intersect in a homoclinic point H (\bullet) generating a complex network of loops.

The future fate and past history of such a homoclinic point is quite interesting. The continuity of the map implies that the iterates $T^n(X)$ of a neighborhood X of a homoclinic point must resemble the original set X , which contains an interval of the manifolds H^+ and H^- . Therefore H^+ and H^- must also cross in each of the iterates $T^n(X)$, $n = 1, 2, \dots$, and we have a series of infinitely many homoclinic points, which are mapped onto each other and converge to the hyperbolic fixed point. Moreover, the map is area-preserving and the area enclosed by the branches of H^+ and H^- between two such homoclinic crossings is equal to the area enclosed by the branches between the subsequent crossings. Unavoidably, this leads to the formation of infinitely many thin loops as a consequence of the forbidden self-crossing of the manifolds. As already stated by Henri Poincaré in 1892,

“The intersections form a kind of lattice, web or network with infinitely tight loops; neither of the two curves (H^+ and H^-) must ever intersect itself but it must bend in such a complex fashion that it intersects all the loops of the network infinitely many times. One is struck by the complexity of this figure which I am not even attempting to draw. Nothing can give us a better idea of the complexity of the three body problem and of all the problems in dynamics. . .” (cited after Tabor [6, p.144]).

It is in the neighborhood of the hyperbolic fixed points that chaotic dynamics can first be observed. With increasing perturbation ε , the destroyed zones grow, and the chaotic area-filling orbits in phase space increase. The ‘chaotic sea’ is, initially, still enveloped by intact invariant tori. With increasing ε , a growing number of invariant tori is destroyed, depending on the irrationality of the frequency ratio.

The last surviving invariant tori are, in most cases, the so-called ‘*noble tori*’, whose frequency ratio is, in some sense, the most irrational (see Sect. 2.4.2 for more details).

Finally, for large perturbation we find wide, extended chaotic regions. Only small islands surrounded by invariant curves remain, which are embedded in the chaotic sea. Sometimes, these islands ultimately disappear and the system becomes ergodic, i.e., almost all trajectories get arbitrarily close to any point on the energy surface.

2.3 Dissipative Dynamical Systems

An important feature of the Hamiltonian systems discussed in the preceding section is the conservation of the volume element in phase space. For a *dissipative system*, this volume element contracts and the trajectory approaches a (lower-dimensional) subset of the phase space, an ‘*attractor*’. Immediately, the problem arises of characterizing the different types of attractors and determining all coexisting attractors dependent on the parameters of the system and the organization of their ‘*basins of attraction*’ in phase space, i.e., the set

of all initial conditions of trajectories converging in the long time limit to a particular attractor, and the structural changes in the attractors when a parameter of the system is varied, i.e., their bifurcation properties.

Let us discuss a few general features of dynamical systems formulated as a system of autonomous differential equations

$$\frac{d\mathbf{x}}{dt} = \mathbf{v}(\mathbf{x}), \quad (2.27)$$

where $\mathbf{x} = (x_1, \dots, x_N)$ is a vector in N -dimensional phase space, and $\mathbf{v} = (v_1, \dots, v_N)$ a vector field in phase space. For a given initial condition $\mathbf{x}_0 = \mathbf{x}(t_0)$, the differential equation (2.27) generates a flow $\mathbf{x}(t) = \mathbf{x}(t, \mathbf{x}_0)$ in phase space. A Poincaré map can be constructed on a surface of section, as illustrated in Fig. 2.2 above, which reduces the dynamics to the study of a discrete dissipative map.

The flow generated by (2.27) contracts the volume element

$$\Delta\tau = \Delta x_1 \Delta x_2 \cdots \Delta x_N \quad (2.28)$$

in phase space at a rate

$$\frac{1}{\Delta\tau} \frac{d\Delta\tau}{dt} = \text{div } \mathbf{v}. \quad (2.29)$$

For some important model systems, this rate is equal to a (negative) constant, $-\gamma$, and the phase space volume elements shrink uniformly in phase space according to $\Delta\tau \sim e^{-\gamma t}$. A well-known example of such a system is the forced and damped harmonic oscillator or, more generally, the Duffing oscillator

$$\ddot{x} + r\dot{x} + \omega_0^2 x + \beta x^3 = f \cos \omega t, \quad (2.30)$$

which is studied in detail in Chap. 8. For $\beta = 0$, we recover the driven harmonic oscillator. This explicitly time-dependent second order differential equation can be rewritten as

$$\begin{aligned} \dot{x} &= v \\ \dot{v} &= -rv - \omega_0^2 x - \beta x^3 + \cos \omega s \\ \dot{s} &= 1, \end{aligned} \quad (2.31)$$

where the introduction of the auxiliary variable s removes the explicit time dependence (note that integration of $\dot{s} = 1$ with $s(0) = 0$ yields $s(t) = t$). The phase space volume contracts at the constant rate

$$\frac{1}{\Delta\tau} \frac{d\Delta\tau}{dt} = \frac{\partial}{\partial x} v + \frac{\partial}{\partial v} (-rv) + \frac{\partial}{\partial s} 1 = -r. \quad (2.32)$$

There are other systems, where the contraction rate varies in phase space, and one can introduce the long time average of the contraction rate along a

trajectory. This is required to be negative for all initial conditions \mathbf{x}_0 for a dissipative system.

For the case of a discrete map

$$\mathbf{x}_{n+1} = \mathbf{f}(\mathbf{x}_n) \quad (2.33)$$

the N -dimensional phase space volume $\Delta\tau$ contracts per iteration by a factor

$$\left| \det \frac{\partial(f_1 \dots f_N)}{\partial(x_1 \dots x_N)} \right|, \quad (2.34)$$

i.e., the Jacobian determinant of the mapping function. For the most famous dissipative map, the one-dimensional logistic map $x_{n+1} = 4r x_n(1 - x_n)$ with $0 \leq x_n \leq 1$, $0 < r < 1$ (see Chap. 9), the contraction per iteration is equal to $4r(1 - 2x_n)$, which is x -dependent and smaller than unity.

2.3.1 Attractors

The attractors in dissipative systems are of special interest. Basically, one can distinguish simple and strange attractors. Two types of simple attractors are already familiar from the driven harmonic oscillator

$$\ddot{x} + r\dot{x} + \omega_0^2 x = f \cos \omega t \quad (2.35)$$

with $r > 0$. For the unforced case $f = 0$, any trajectory converges to the stationary solution $x = 0$, a ‘*limit point*’ or ‘*point attractor*’. For the driven case, $f \neq 0$, the function

$$x(t) = A \cos(\omega t - \phi) \quad (2.36)$$

— with an amplitude $A = f\{(\omega_0^2 - \omega^2)^2 + (r\omega)^2\}^{-1/2}$ and a phase shift given by $\phi = r\omega/(\omega_0^2 - \omega^2)$ — is a periodic solution oscillating with the same period as the external excitation. Any solution converges in the long time limit to (2.36) as illustrated in Fig. 2.7. Such an attracting periodic solution is called a ‘*limit cycle*’.

For the harmonic oscillator there is only one limit cycle, but for nonlinear systems as, for example, the Duffing oscillator (2.30), various limit cycles may coexist. This is explored in more detail in Chap. 8. In addition, the period of the limit cycle may be entirely determined by intrinsic properties of the system, and not by any external driving function. Other simple attractors are two-dimensional tori embedded in phase space and supporting a limiting quasiperiodic oscillation characterized by two frequencies.

When a parameter of the systems is varied slowly, the attracting limit points and limit cycles also change, while remaining structurally similar. At certain critical values, however, they can undergo sudden changes, e.g., change their character, split into pairs, disappear, etc. Such phenomena are called ‘*bifurcations*’. A characteristic example is the so-called ‘*Hopf bifurcation*’, where a limit point changes into a limit cycle (see Sect. 2.4.6 for more details).

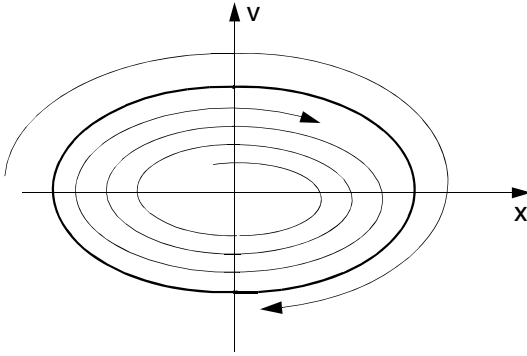


Fig. 2.7. Attracting limit cycle for the damped and driven harmonic oscillator.

A ‘*strange attractor*’ is a limit set, which is much more complicated [12]. First, it is a fractal object, characterized by a noninteger, fractal dimension. A strange attractor has self-similar properties, i.e., a magnification of a part of it is similar to the whole set. Secondly, the dynamics *on* the strange attractor is chaotic, and characterized by an extreme sensitivity to small changes in the initial conditions. Nearby trajectories diverge exponentially, which can be quantitatively measured by the ‘*Lyapunov exponent*’, as described in more detail in Sect. 2.4.3. Both the non-trivial geometry and the irregular dynamics will be explored by means of computer experiments in the following chapters, in Chap. 8 and Chap. 12 in particular.

The two characteristic features, namely ‘exponential divergence of neighboring trajectories’ and ‘contraction of phase space’, seem to be incompatible at first sight and, in fact, they can not simultaneously occur in two-dimensional phase space. For $N \geq 3$, however, such chaotic dissipative dynamics is possible. This can be understood using a simple model: a thin band of trajectories in three-dimensional phase space is first stretched (exponential divergence) and compressed (phase space contraction). It is then folded over and re-injected into itself, as illustrated in Fig. 2.8. This process is then iterated. It should be

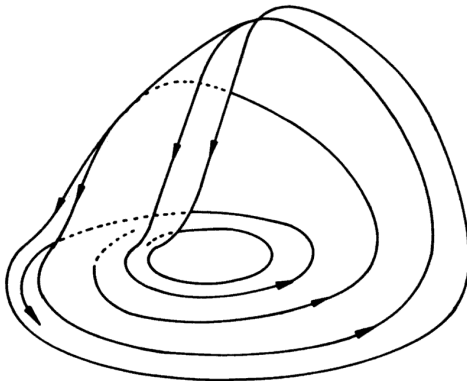


Fig. 2.8. Dissipative flow in three-dimensional phase space converging to a strange attractor.

noted that phase space trajectories can not cross and that the limiting set of this process will be a very complicated geometrical object.

The process of stretching and folding can be illustrated by the ‘*Smale horseshoe map*’ [13]. The map consists of a *stretching* of a two-dimensional square followed by a folding over into the shape of a horseshoe, as illustrated in Fig. 2.9. This defines a map of the square onto itself, which contracts the area and separates nearby points. When this process is iterated, a very complex set of points is generated. A vertical section through the square reveals that the set consists of 2^n disjoint segments after n iterations. Mathematically, such a limiting set is called a ‘*Cantor set*’, i.e., a compact, uncountable, and totally disconnected set, a ‘*fractal*’ object, which can be characterized by a non-integer dimension.

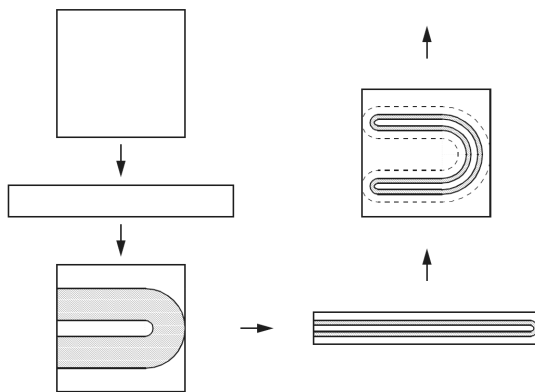


Fig. 2.9. Illustration of the Smale horseshoe map of a square, which consists of a stretching and a compression of the area followed by a folding over. This process is iterated.

2.3.2 Routes to Chaos

When the external parameters of a system are varied, the dynamical behavior can change in character. In particular, it is of interest to study the transition from a parameter region with regular dynamics to a chaotic regime. Several characteristic routes of a system from regularity to chaos have been observed. Such a route is called a ‘*scenario*’.

An example is the ‘*Poincaré scenario*’ in Hamiltonian systems, which is characterized by the consecutive destruction of invariant tori according to their degree of ‘rationality’, as described in the preceding section. For dissipative systems other scenarios are known and, to some extent, understood, but the full theory of the transition to chaos has still to be developed.

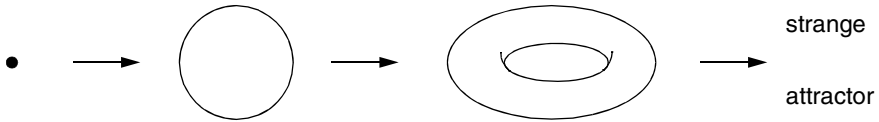


Fig. 2.10. The Ruelle-Takens-Newhouse scenario: bifurcation of attractors in phase space.

The ‘*period-doubling scenario*’ consists of a sequence of period-doubling bifurcations (see Sect. 2.4.6), where a stable periodic orbit becomes unstable, while a stable orbit of period two is born, which bifurcates again into a four-periodic orbit and so on. Finally, after an infinite number of such bifurcations, the system becomes chaotic.

Another important route to chaos is the ‘*Ruelle-Takens-Newhouse scenario*’ [14, 15], which is characterized by a sequence of three bifurcations, as illustrated in Fig. 2.10. First, we find a point attractor, i.e., the system approaches a stable equilibrium. For a critical parameter value, this point attractor turns into a limit cycle (a Hopf bifurcation, as discussed in Sect. 2.4.6) and the system oscillates periodically. After a further parameter change, this periodic orbit loses its stability and bifurcates into a two-dimensional torus attractor in phase space (see Fig. 2.10). The motion on the attractor is quasiperiodic, characterized by two frequencies related to the two different rotations on the torus. When this torus-attractor is destabilized by a further parameter change, it turns into a strange attractor.

Finally, a system can become chaotic via the ‘*intermittency*’ route, as proposed by Manneville and Pomeau [16, 17]. Such intermittent behavior can most easily be discussed in terms of one-dimensional maps (see Sect. 2.4.4). A stable fixed point, i.e., a point attractor, and an unstable fixed point approach each other when a parameter is varied. At a critical point they coalesce and disappear. In this region the system shows characteristic intermittent behavior, an almost regular and seemingly organized dynamics in the vicinity of the destroyed fixed point interrupted by long intervals of irregular motion (see Sects. 2.4.4 and 2.4.6 for more details).

2.4 Special Topics

In order to assist the reader in a somewhat deeper analysis of the computer experiments, we present in this section some more specialized topics in nonlinear dynamics, which will be useful in many of the systems studied in the following computer experiments. The material is, however, slightly more technical and the connection and relevance to chaotic dynamics is not directly obvious. This section can be omitted at a first reading.

2.4.1 The Poincaré-Birkhoff Theorem

According to the KAM theorem for Hamiltonian systems with two degrees of freedom (see Sect. 2.2) invariant tori with a sufficiently irrational ratio of the two basic frequencies ω_1/ω_2 remain invariant under a small perturbation of the Hamiltonian. Tori with a rational frequency ratio are excluded by the conditions of the KAM theorem and are, in most cases, destroyed.

Let us consider this rational case in more detail. For convenience, we consider a two-dimensional mapping of the plane, which models, for example, a Poincaré map of a two-dimensional Hamiltonian H_0 :

$$\begin{aligned}\rho_{i+1} &= \rho_i \\ \theta_{i+1} &= \theta_i + 2\pi\alpha(\rho_i),\end{aligned}\tag{2.37}$$

or simply

$$\begin{pmatrix} \rho_{i+1} \\ \theta_{i+1} \end{pmatrix} = \mathbf{T} \begin{pmatrix} \rho_i \\ \theta_i \end{pmatrix}.\tag{2.38}$$

The mapping \mathbf{T} is called a ‘*twist map*’, where the radial coordinate ρ and the angular coordinate θ model action-angle variables, and α plays the role of the frequency ratio. The mapping is area-preserving:

$$\left| \frac{\partial(\rho_{i+1}, \theta_{i+1})}{\partial(\rho_i, \theta_i)} \right| = \left| \begin{array}{cc} 1 & 0 \\ 2\pi\alpha'(\rho_i) & 1 \end{array} \right| = 1\tag{2.39}$$

($\alpha' = d\alpha/d\rho$). The dynamics of the twist map is simple. The radial coordinate ρ is conserved and all points move along concentric circles, where the winding number α varies with the radius. For circles with a rational α -value

$$\alpha = r/s,\tag{2.40}$$

all points are s -periodic, i.e., fixed points of \mathbf{T}^s . If the twist map (2.37) is perturbed as

$$\begin{aligned}\rho_{i+1} &= \rho_i + \epsilon f(\rho_i, \theta_i) \\ \theta_{i+1} &= \theta_i + 2\pi\alpha(\rho_i) + \epsilon g(\rho_i, \theta_i),\end{aligned}\tag{2.41}$$

where the (sufficiently well-behaved) functions f and g are chosen so that the mapping

$$\begin{pmatrix} \rho_{i+1} \\ \theta_{i+1} \end{pmatrix} = \mathbf{T}_\epsilon \begin{pmatrix} \rho_i \\ \theta_i \end{pmatrix}.\tag{2.42}$$

is still area-preserving, the perturbed map \mathbf{T}_ϵ can again be considered as a Poincaré map generated by a Hamiltonian $H_0 + \epsilon H_1$. The KAM theorem then guarantees that the invariant circles of \mathbf{T} having a sufficiently irrational value of α are slightly transformed invariant curves of \mathbf{T}_ϵ for small values of ϵ .

The *Poincaré-Birkhoff theorem* [18] states that invariant circles with *rational* values $\alpha = r/s$ (r and s are coprime integer numbers) consisting entirely of fixed points of \mathbf{T} are not completely destroyed. A number of $2ks$ points, $k \in \mathbb{N}$, transform into fixed points of \mathbf{T}_ϵ^s . Half of these fixed points are elliptic and half are hyperbolic, forming an alternating chain (a short outline of the proof can be found in Ref. [4] or [19]). The schematic illustration in Fig. 2.11 shows two destroyed invariant curves with $\alpha = 1/3$ and $1/4$ forming chains of three and four elliptic and hyperbolic fixed points, respectively.

The vicinity of the hyperbolic fixed points show the complex irregular dynamics governed by the homoclinic tangle described in Sect. 2.2.4 above. Let us now explore the neighborhood of the elliptic fixed points of the chain \mathbf{T}_ϵ^s in more detail. At first sight, these ‘small’ fixed points seem to be surrounded by invariant curves. This is, however, an illusion. As before, the KAM and Poincaré-Birkhoff theorems can now be applied to the ‘small’ elliptic fixed points, showing that the seemingly invariant curves encircling them are also broken up into alternating elliptic and hyperbolic fixed points for rational rotation numbers. Figure 2.11 shows, for example, a magnification of such a region. Repeating this process by again magnifying the magnified fixed points reveals a fascinating self-similar structure of the phase space down to an arbitrarily small scale, as illustrated in Fig. 2.11.

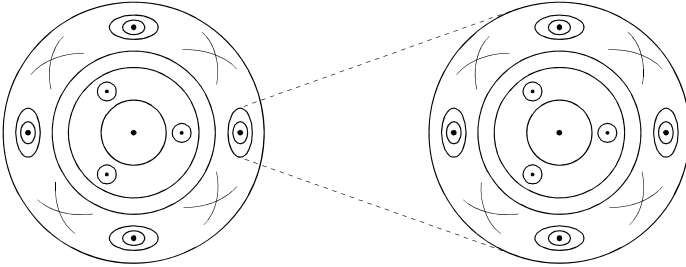


Fig. 2.11. Decay of invariant curves into chains of alternating elliptic and hyperbolic fixed points leading to a self-similar structure of the phase space.

2.4.2 Continued Fractions

The behavior of dynamical systems is, in many cases, sensitively dependent on the number-theoretic character of the value of certain parameters. To take an example, in the study of billiard systems in Chap. 3, an increasing deformation of the regular circular billiard with quasiperiodic motion destroys an increasing fraction of these regular orbits, depending on the irrationality of the quasi-periodicity. The KAM theorem requires that a frequency ratio be ‘sufficiently irrational’. It is therefore necessary to gain some understanding of the relationship between rational and real numbers.

As is well known, a real number x can be arbitrarily closely approximated by rational numbers r/s . Here and in the following, r and s are coprime integers. The most familiar rational approximation is the decimal expansion, e.g.

$$\pi = 3.141592654 \dots \approx \frac{3}{1}, \frac{31}{10}, \frac{314}{100}, \dots \quad (2.43)$$

The quality of the decimal approximation is given by

$$\left| x - \frac{r}{s} \right| < \frac{1}{s} \quad (2.44)$$

and the approach is one-sided, i.e., the rational approximations are always smaller or larger than x for $x > 0$ or $x < 0$, respectively.

Let us now discuss the continued fraction expansion of a real number x :

$$x = a_0 + \frac{1}{a_1 + \frac{1}{a_2 + \frac{1}{a_3 + \dots}}}, \quad (2.45)$$

($a_0 \in \mathbb{Z}$, $a_1, a_2, \dots \in \mathbb{N}$). This expansion is unique and can easily be constructed for any x by taking a_0 as the integer part of x , defining

$$x_0 = x - a_0 \quad , \quad a_1 = [x_0^{-1}], \quad (2.46)$$

where the Gauss bracket $[\]$ denotes the largest integer number less than or equal to the real number inside. Iterating the construction (2.46)

$$x_n = x_{n-1}^{-1} - a_n \quad , \quad a_{n+1} = [x_n^{-1}], \quad n = 1, 2, \dots \quad (2.47)$$

yields the series of the integers a_n .

The series of rational numbers obtained by cutting the continued fraction expansion (2.45) at a_n defines a series of rational approximations

$$x \approx \frac{r_0}{s_0}, \frac{r_1}{s_1}, \dots, \frac{r_n}{s_n}, \dots \quad (2.48)$$

Such a r_n/s_n is the *best* rational approximation of x , i.e., there is no rational number with $s < s_n$ and

$$\left| x - \frac{r}{s} \right| < \left| x - \frac{r_n}{s_n} \right|. \quad (2.49)$$

A well-known example of such an approximation in terms of continued fractions is the series

$$\pi \approx \frac{3}{1}, \frac{22}{7}, \frac{333}{106}, \frac{355}{113}, \dots \quad (2.50)$$

It can be shown that the quality of the continued fraction approximation is given by

$$\left| x - \frac{r_n}{s_n} \right| < \frac{1}{s_n s_{n-1}}, \quad (2.51)$$

which is much stronger than, for example, the quality of the simple decimal approximation (2.43). In addition, the convergence is alternating, i.e., x lies between two subsequent approximations.

From (2.45), we see that the convergence of the continued fraction approximation is better for larger values of the natural numbers a_n . The slowest convergence is evidently found for $a_1 = a_2 = \dots = 1$, corresponding to

$$g^* = \frac{1}{1 + \frac{1}{1 + \frac{1}{1 + \dots}}}, \quad (2.52)$$

which is least well approximated by the rational numbers. g^* is the so-called ‘golden number’, ‘golden mean’, or ‘golden ratio’. It is closely related to the ‘Fibonacci numbers’

$$\{F_n\} = \{0, 1, 1, 2, 3, 5, 8, 13, \dots\}, \quad (2.53)$$

which are defined by the recursion $F_{n+1} = F_n + F_{n-1}$ with $F_0 = 0$, $F_1 = 1$. From the ratio

$$u_n = \frac{F_n}{F_{n+1}} = \frac{F_n}{F_n + F_{n-1}} = \frac{1}{1 + u_{n-1}} \quad (2.54)$$

and $u_0 = 0$ we recover by iteration the continued fraction expansion (2.52) and, in addition,

$$g^* = \lim_{n \rightarrow \infty} u_n = \lim_{n \rightarrow \infty} \frac{1}{1 + u_{n-1}} = \frac{1}{1 + g^*}. \quad (2.55)$$

This yields the quadratic equation $g^*(1 + g^*) = 1$ having the solution

$$g^* = \frac{1}{2} (\sqrt{5} - 1) = 0.61803\dots, \quad (2.56)$$

which is known as the ‘golden mean’. This number can be considered as the ‘most irrational’ number in the interval $[0, 1]$. In fact, there is a whole class of similar numbers, where the continued fraction expansion has the form

$$\{a_0, a_1, \dots, 1, 1, 1, \dots\}. \quad (2.57)$$

Such numbers are called ‘noble numbers’. The most important noble numbers in the interval $[0, 1]$ are those of the form

$$g_k^* = \frac{1}{k + g^*}, \quad k = 1, 2, \dots, \quad (2.58)$$

with $g_1^* = g^*$, $g_2 = 1/(2 + g^*) = 1 - g^* \approx 0.38197\dots$

As an example, we consider the perturbed two-dimensional Hamiltonian system discussed in Sect. 2.2.3, where the KAM theorem guarantees the preservation of all invariant tori, whose frequency ratio satisfies

$$\left| \frac{\omega_1}{\omega_2} - \frac{r}{s} \right| > \frac{K(\varepsilon)}{s^{5/2}}, \quad (2.59)$$

i.e., whose frequency ratio is sufficiently irrational. With increasing perturbation these zones shrink to zero until finally all invariant tori are destroyed. The last invariant tori are, in many cases, those whose frequency ratio equals a noble number, the so-called ‘*noble tori*’ (compare, e.g., the numerical experiment for the double pendulum in Sect. 5.4.3).

2.4.3 The Lyapunov Exponent

Chaotic dynamics is characterized by an exponential divergence of initially close points. Let us first discuss the case of one-dimensional discrete maps of an interval

$$x_{n+1} = f(x_n), \quad x \in [0, 1], \quad (2.60)$$

which are studied numerically in Chap. 9. The so-called ‘*Lyapunov exponent*’ is a measure of the divergence of two orbits starting with slightly different initial conditions x_0 and $x_0 + \Delta x_0$. The distance after n iterations

$$\Delta x_n = |f^n(x_0 + \Delta x_0) - f^n(x_0)| \quad (2.61)$$

increases exponentially for large n for a chaotic orbit according to

$$\Delta x_n \approx \Delta x_0 e^{\lambda_L n}. \quad (2.62)$$

One can now relate the Lyapunov exponent analytically to the average stretching along the orbit $x_0, x_1 = f(x_0), x_2 = f(f(x_0)), \dots, x_n = f^n(x_0) = f(f(f \dots (x_0) \dots))$. From (2.61) and the chain rule of differentiation, we have

$$\begin{aligned} \ln \frac{\Delta x_n}{\Delta x_0} &\approx \ln \left| \frac{f^n(x_0 + \Delta x_0) - f^n(x_0)}{\Delta x_0} \right| \\ &\approx \ln \left| \frac{df^n(x)}{dx} \right| = \ln \prod_{j=0}^{n-1} |f'(x_j)| \\ &= \sum_{j=0}^{n-1} \ln |f'(x_j)|, \end{aligned} \quad (2.63)$$

and finally

$$\lambda_L = \lim_{n \rightarrow \infty} \frac{1}{n} \ln \frac{\Delta x_n}{\Delta x_0} = \lim_{n \rightarrow \infty} \frac{1}{n} \sum_{j=0}^{n-1} \ln |f'(x_j)|, \quad (2.64)$$

where the logarithm of the linearized map is averaged over the orbit x_0, x_1, \dots, x_{n-1} .

Negative values of the Lyapunov exponent indicate stability, and positive values chaotic evolution, where λ_L measures the speed of exponential divergence of neighboring trajectories. At critical bifurcation points the Lyapunov exponent is zero.

For an interpretation of the Lyapunov exponent, it is instructive to note its relationship to the loss of information during the process of iteration. When the interval $[0, 1]$ is partitioned into N equal boxes, one needs $\text{ld } N$ bits of information (ld is the logarithm of base two) to localize the particular box containing the point x_j , i.e., one has to ask $\text{ld } N$ ‘yes’ or ‘no’ questions on average. After an iteration this box is stretched by a factor $|f'(x_j)|$ and we have an information loss

$$\Delta I(x_j) = -\text{ld } |f'(x_j)| \quad (2.65)$$

regarding the position of the iterated point. The Lyapunov exponent can therefore be interpreted as the average loss of information:

$$\lambda_L = -\ln 2 \lim_{n \rightarrow \infty} \frac{1}{n} \sum_{j=0}^{n-1} \Delta I(x_j) = -\ln 2 \overline{\Delta I(x_j)}, \quad (2.66)$$

where the factor $\ln 2$ converts binary (‘bits’) to natural (‘nats’) units of information.

It is also of interest to express the Lyapunov exponent in terms of the asymptotic density of points covered by the orbit x_0, x_1, x_2, \dots

$$\varrho(x) = \lim_{n \rightarrow \infty} \frac{1}{n} \sum_{j=0}^{n-1} \delta(x - x_j), \quad (2.67)$$

which is, by virtue of its construction, invariant under the mapping function $f(x)$. This ‘*invariant density*’ satisfies the integral equation

$$\varrho(x) = \int dx' \varrho(x') \delta(x - f(x')) \quad (2.68)$$

and from (2.67) we directly find the identity

$$\lambda_L = \int dx \varrho(x) \ln |f'(x)|. \quad (2.69)$$

In view of (2.66), this expression strongly resembles the usual definition of an (information theoretic) entropy, $\ln |f'(x)|$, averaged over the probability distribution.

The above discussion of the Lyapunov exponent as a quantitative measure of the average exponential separation of neighboring orbits can be extended to

higher dimensional discrete mappings and to continuous flows. Let us discuss, for example, a Hamiltonian system in $2N$ -dimensional phase space $(\mathbf{p}(t), \mathbf{q}(t))$ evolving from an initial point $(\mathbf{p}(t_0), \mathbf{q}(t_0))$. Let us denote this orbit as the ‘reference orbit’. We now follow a slightly displaced orbit, whose starting point is shifted by a small amount $(\Delta\mathbf{p}(t_0), \Delta\mathbf{q}(t_0))$. The time evolution of the separation from the reference orbit can be expressed in terms of the stability matrix $\mathbf{M}(t, t_0)$ connecting the distance in $(\Delta\mathbf{p}(t), \Delta\mathbf{q}(t))$ at time t with the separation at time t_0 :

$$(\Delta\mathbf{p}(t), \Delta\mathbf{q}(t)) = \mathbf{M}(t, t_0)(\Delta\mathbf{p}(t_0), \Delta\mathbf{q}(t_0)). \quad (2.70)$$

The Lyapunov exponent is defined as the long time limit

$$\lambda_L = \lim_{t \rightarrow \infty} \frac{\ln \|\mathbf{M}(t, t_0)\|}{t - t_0}, \quad (2.71)$$

where $\|\mathbf{M}\|$ denotes a matrix norm. For a regular trajectory the separation of neighboring trajectories grows as a (low) power of t , i.e., less than exponentially, and the Lyapunov exponent is zero. A positive Lyapunov exponent characterizes a chaotic trajectory. Typically, such a trajectory covers a certain phase space region and the Lyapunov exponent characterizes this region, regardless of the initial condition.

In many practical problems, however, a computation of λ_L using this equation is not practicable because of two problems: first, the exponential growth (2.71) may lead to numerical errors and computer overflow. Second, it can not hold for all times, simply because in many cases the accessible phase space is bounded.

These problems can be overcome by using a repeated rescaling of the offset from the reference trajectory (see Fig. 2.12). Starting at time $t_0 = 0$ with a displaced orbit at a distance

$$d_0 = |(\Delta\mathbf{p}(0), \Delta\mathbf{q}(0))| \quad (2.72)$$

from the reference orbit, we follow this orbit for a time interval τ , compute the new distance

$$d_1 = |(\Delta\mathbf{p}(\tau), \Delta\mathbf{q}(\tau))|, \quad (2.73)$$

and start a new displaced trajectory at the rescaled initial point

$$(\mathbf{p}(\tau), \mathbf{q}(\tau)) + \frac{d_0}{d_1}(\Delta\mathbf{p}(\tau), \Delta\mathbf{q}(\tau)). \quad (2.74)$$

The trajectory is followed up to time $t = 2\tau$, the new deviation

$$d_2 = |(\Delta\mathbf{p}(2\tau), \Delta\mathbf{q}(2\tau))|, \quad (2.75)$$

is computed, and a second rescaled trajectory is started. This process is continued, yielding a sequence of scaling factors d_0, d_1, d_2, \dots from which the Lyapunov exponent can be computed as

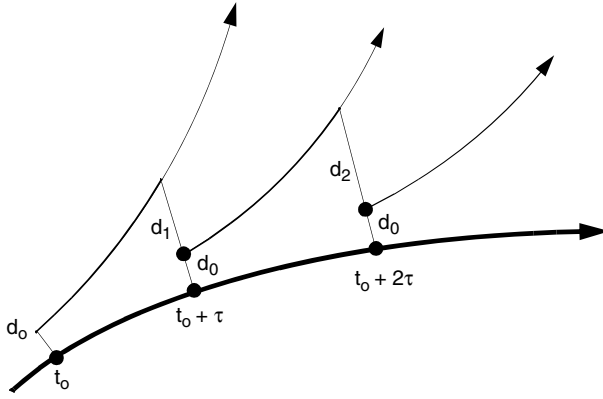


Fig. 2.12. Computation of the Lyapunov exponent by repeated rescaling of the distance of a displaced trajectory from a reference orbit.

$$\lambda_L = \lim_{n \rightarrow \infty} \frac{1}{n\tau} \sum_{n=1}^n \ln \frac{d_n}{d_0}. \quad (2.76)$$

2.4.4 Fixed Points of One-Dimensional Maps

The dynamics of one-dimensional mappings

$$x_{n+1} = f(x_n, r), \quad (2.77)$$

where r is a parameter, may converge in the long-time limit to the fixed points

$$x^* = f(x^*, r). \quad (2.78)$$

The stability of a fixed point x^* can be obtained from linearization of the map (2.77) in the vicinity of the fixed point:

$$x_{n+1} - x^* = f'(x^*, r) (x_n - x^*) \quad (2.79)$$

with $f' = df/dx$. This implies that deviations from the fixed point shrink for

$$|f'(x^*, r)| < 1 \quad (\text{stable fixed point}) \quad (2.80)$$

and magnify for

$$|f'(x^*, r)| > 1 \quad (\text{unstable fixed point}). \quad (2.81)$$

In the case $|f'(x^*, r)| = 1$ we have neutral stability.

It is important to realize that this simple criterion also applies to the stability of periodic k -cycles

$$x_0, x_1, \dots, x_k = x_0$$

with $x_n = f(x_{n-1}, r)$. Each member of this k -cycle is a fixed point x^* of the k -times iterated map

$$x^* = f^k(x^*, r) = \underbrace{f(\dots f(x^*, r) \dots)}_{k\text{-times}} \quad (2.82)$$

and the chain rule for differentiation yields

$$\left| \frac{df^k}{dx} \right|_{x^*} = \prod_{n=0}^{k-1} |f'(x_n, r)| \quad \begin{cases} < 1 & \text{stable fixed point} \\ > 1 & \text{unstable fixed point} \end{cases}, \quad (2.83)$$

for $x^* = x_n$, $n = 0, \dots, k-1$.

It is evident from (2.83) that the slope of f^k is identical for all k members x_n , $n = 0, \dots, k-1$ of the k -periodic orbit. Graphically, this means that the function $f^k(x)$ becomes simultaneously tangential to the bisector $y(x) = x$ for the whole chain of fixed points when this orbit loses stability.

Let us look at the loss of stability of a fixed point $x^* = f(x^*, r)$ in more detail. Increasing the parameter r from a stable region ($|f'(x^*, r)| < 1$) to an unstable region ($|f'(x^*, r)| > 1$) crossing a critical value r_1 with $|f'(x^*, r_1)| = 1$, the fixed point $x^* = x^*(r)$ becomes unstable at $r = r_1$. We note that any fixed point of f is also a fixed point of the iterated map f^2 having the same stability properties. However, at $r = r_1$ a stable period-two orbit (x_-^*, x_+^*) with

$$x_-^* \xrightarrow{f} x_+^* \xrightarrow{f} x_-^*, \quad (2.84)$$

is born. Both points, x_-^* and x_+^* , are stable fixed points of the iterated map f^2 , i.e., the slope of f^2 is smaller than unity:

$$\begin{aligned} \left| \frac{df^2}{dx} \right|_{\{x_{\pm}^*\}} &= \left| \frac{df^2}{dx} \right|_{\{x_{\pm}^*\}} \\ &= |f'(x_-^*, r)| |f'(x_+^*, r)| < 1, \end{aligned} \quad (2.85)$$

provided that r is close enough to r_1 . This bifurcation of fixed points — a so-called ‘pitchfork bifurcation’ — is illustrated in Figs. 2.13 and 2.14. It is investigated numerically in Chap. 9.

For increasing values of the parameter r , the fixed points of f^2 can also lose their stability at r_2 and bifurcate again into period-four orbits (fixed points of f^4), and so on.

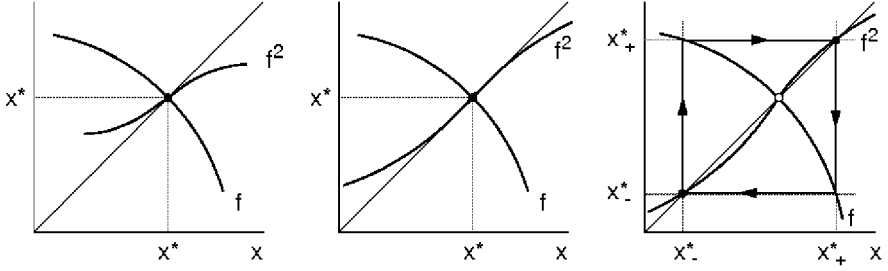


Fig. 2.13. Pitchfork bifurcation: A stable period-one fixed point x^* loses stability at a critical value of the parameter $r = r_1$, where the slope $|f'(x^*)|$ is unity, and a pair of period-two fixed points x_-^* and x_+^* is born.

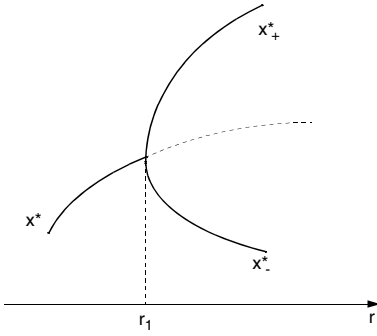


Fig. 2.14. Pitchfork bifurcation: A stable period-one fixed point x^* loses stability at a critical value of the parameter $r = r_1$ and a pair of period-two fixed points x_-^* and x_+^* is born. The dashed curve marks the position of the unstable fixed point x^* .

Another bifurcation of fixed points of one-dimensional maps can be observed when the mapping function $f(x, r)$ becomes tangential to the bisector at a critical parameter value r_c , as illustrated in Fig. 2.15. For, say, $r > r_c$ we have two intersections with the bisector, $x^* = f(x^*, r)$, i.e., two fixed points of the map. At the critical parameter, the slope of f is unity and therefore one of the fixed points is stable (slope smaller than unity) and one is unstable (slope larger than unity). In the limit $r \rightarrow r_c$ the fixed points approach each other. They coalesce at r_c , and disappear for $r > r_c$. This bifurcation is called a ‘*tangent bifurcation*’.

For $r \gtrsim r_c$ there is a narrow channel between the mapping function and the bisector. When the iterates enter this channel, it takes a large number of iterations until the iterates are ejected from it again. During this process, the behavior of the iterates is very regular, but outside the channel the iteration may be irregular until the channel is re-entered. This behavior is called ‘*intermittency*’ [16, 17].

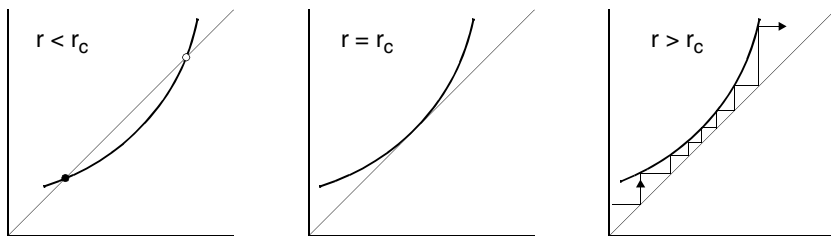


Fig. 2.15. Tangent bifurcation and intermittency: A stable (●) and an unstable (○) fixed point coalesce and disappear at a critical parameter value r_c .

2.4.5 Fixed Points of Two-Dimensional Maps

Two-dimensional discrete maps

$$\begin{aligned} x_{n+1} &= f(x_n, y_n) \\ y_{n+1} &= g(x_n, y_n) \end{aligned} \quad (2.86)$$

are important models for studying chaotic dynamics. A popular example is the Mandelbrot map explored in detail in Chap. 11. Such maps constitute interesting dynamical systems, which may be analyzed without any obvious physical interpretation. They may appear in a direct way, modeling, e.g., periodically kicked systems (see Chap. 13), or they can appear as Poincaré maps of higher dimensional flows. An example are Hamiltonian systems with two degrees of freedom, whose dynamics in four-dimensional phase space is often reduced to the study of area-preserving two-dimensional Poincaré maps, which form an important subclass of two-dimensional maps.

Dissipative Maps: The stability and bifurcation properties of two-dimensional maps are much richer than in the one-dimensional case. Let us consider a fixed point (x^*, y^*) of the map (2.86), so that

$$\begin{aligned} x^* &= f(x^*, y^*) \\ y^* &= g(x^*, y^*). \end{aligned} \quad (2.87)$$

We can investigate the stability properties at the fixed point by means of a two-dimensional Taylor expansion

$$\begin{aligned} x_{n+1} &\approx f(x^*, y^*) + \left. \frac{\partial f}{\partial x} \right|_* (x_n - x^*) + \left. \frac{\partial f}{\partial y} \right|_* (y_n - y^*) \\ y_{n+1} &\approx g(x^*, y^*) + \left. \frac{\partial g}{\partial x} \right|_* (x_n - x^*) + \left. \frac{\partial g}{\partial y} \right|_* (y_n - y^*) \end{aligned} \quad (2.88)$$

(here, a subscript $*$ denotes that the derivative is evaluated at the fixed point). We rewrite the linearized map in matrix form as

$$\begin{pmatrix} x_{n+1} - x^* \\ y_{n+1} - y^* \end{pmatrix} \begin{pmatrix} \partial f/\partial x|_* & \partial f/\partial y|_* \\ \partial g/\partial x|_* & \partial g/\partial y|_* \end{pmatrix} \begin{pmatrix} x_n - x^* \\ y_n - y^* \end{pmatrix} \quad (2.89)$$

or, by introducing the deviation vector $\boldsymbol{\xi}$ with components $\xi_x = x - x^*$ and $\xi_y = y - y^*$, as

$$\boldsymbol{\xi}_{n+1} = \mathbf{L} \boldsymbol{\xi}_n \quad (2.90)$$

with

$$\mathbf{L} = \begin{pmatrix} \partial f/\partial x|_* & \partial f/\partial y|_* \\ \partial g/\partial x|_* & \partial g/\partial y|_* \end{pmatrix} = \left. \frac{\partial(f, g)}{\partial(x, y)} \right|_*. \quad (2.91)$$

The eigenvalues of the matrix \mathbf{L} are given by

$$\lambda_{\pm} = \frac{1}{2} \left\{ \text{Tr } \mathbf{L} \pm \sqrt{(\text{Tr } \mathbf{L})^2 - 4 \det \mathbf{L}} \right\} \quad (2.92)$$

(with $\text{Tr } \mathbf{L} = L_{11} - L_{22}$ and $\det \mathbf{L} = L_{11}L_{22} - L_{12}L_{21}$), which are interrelated by

$$\begin{aligned} \lambda_+ + \lambda_- &= \text{Tr } \mathbf{L}, \\ \lambda_+ \lambda_- &= \det \mathbf{L}. \end{aligned} \quad (2.93)$$

The eigenvalues therefore depend on two real valued parameters $\det \mathbf{L}$ and $\text{Tr } \mathbf{L}$, and the character of the fixed point can be conveniently related to different regions in the $(\det \mathbf{L}, \text{Tr } \mathbf{L})$ -plane. This is discussed below.

There are two possibilities, as is obvious from (2.93): both eigenvalues λ_{\pm} can be real or complex conjugate. These two cases are separated by the parabola

$$(\text{Tr } \mathbf{L})^2 = 4 \det \mathbf{L} \quad (2.94)$$

in the $(\det \mathbf{L}, \text{Tr } \mathbf{L})$ -plane.

If both eigenvalues are inside the unit circle $|\lambda_{\pm}| < 1$ the magnitude of the difference vector contracts, the iterates of the linearized map converge to $\boldsymbol{\xi} = 0$, and the fixed point is stable. The stability region in the $(\det \mathbf{L}, \text{Tr } \mathbf{L})$ -plane is a triangle bounded by the three straight-lines

$$\text{Tr } \mathbf{L} - \det \mathbf{L} = 1, \quad \text{Tr } \mathbf{L} + \det \mathbf{L} = -1, \quad \text{and} \quad \det \mathbf{L} = 1. \quad (2.95)$$

When parameters of the system are varied so that one or two eigenvalues cross the stability boundary $\lambda = 1$, characteristic bifurcations occur. One can distinguish three possibilities, depending on the crossed boundary line of the stability triangle:

- (a) a so-called ‘*divergence*’ occurs on the line $\text{Tr } \mathbf{L} - \det \mathbf{L} = 1$,
- (b) a ‘*flip*’ on the line $\text{Tr } \mathbf{L} + \det \mathbf{L} = -1$, and
- (c) a ‘*flutter*’ or ‘*Neimark bifurcation*’ on the line $\det \mathbf{L} = 1$.

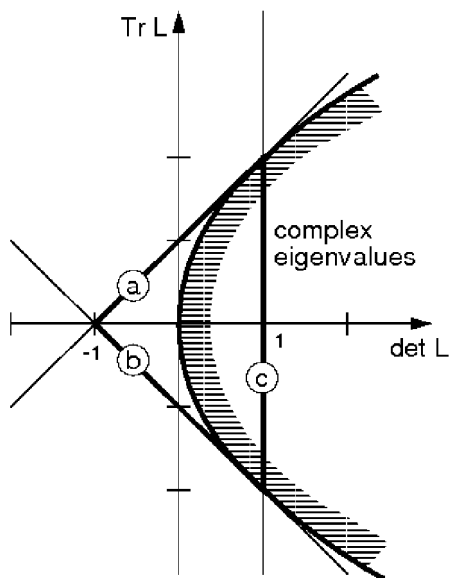


Fig. 2.16. Stability of a two-dimensional map L . Crossing the boundary of the stability triangle leads to characteristic bifurcations. In the convex region bounded by the dashed line the eigenvalues are complex conjugate.

In the first two cases, (a) and (b), the eigenvalues are real and — because of the inequality $|\lambda_+ \lambda_-| < 1$ — only a single eigenvalue, e.g., λ_+ , can cross the unit circle and the other eigenvalue, λ_- , must be smaller than one in magnitude. Therefore, the dynamics of the iterates is basically one-dimensional: the iterates of the map first approach a line (contraction because of $|\lambda_-| < 1$) and then converge along this line to the center $\xi = 0$ in the case of stability, or diverge to infinity in the case of instability. The details depend on the character of the crossing, $\lambda = +1$ for a linear divergence or $\lambda = -1$ for a linear flip, as well as on the sign of the second eigenvalue.

For case (c) — a linear ‘flutter’ or ‘Neimark’ bifurcation — the behavior is more involved. Here, a pair of complex conjugate eigenvalues crosses the unit circle $|\lambda_{\pm}| = 1$ simultaneously. The real part of the eigenvalues are identical and two cases can be distinguished:

- For a crossing with a positive real part, the iterates spiral inward in the stable region and outward in the case of instability. Exactly at the crossing we have neutral stability and the iterates trace out an elliptic orbit.
- For a negative real part, the iterates spiral and oscillate simultaneously. In addition, the behavior can be sensitively dependent on the phase of the eigenvalues at the crossing point of the unit circle. A rational phase $2\pi r/s$ leads to an s -periodic rotation (because of $\lambda^s = 1$) tracing out an elliptic

orbit, which slowly contracts (inside the stability region) or expands (outside the stability region).

The interested reader can investigate these bifurcations numerically in some of the computer experiments described below (most directly for the two-dimensional maps studied in Chap. 11). More details about the theoretical description can be found in Ref. [3, Sect. 8.4].

Area-Preserving Maps: In the remainder of this section we will discuss the special case of Hamiltonian dynamics. Here, the phase space volume is preserved, we find area-preserving maps and the linearized mapping (2.90) is restricted by

$$\det \mathbf{L} = 1. \quad (2.96)$$

Therefore, the eigenvalues λ_{\pm} of \mathbf{L} must satisfy $\lambda_+ \lambda_- = 1$ and the stability properties depend on the value of $\text{Tr } \mathbf{L}$. Two cases can be distinguished:

(a) $|\text{Tr } \mathbf{L}| > 2$: In this case the eigenvalues are real. Let us first assume $\text{Tr } \mathbf{L} > 2$. We then have $\lambda_+ > \lambda_- > 0$ and the eigenvalues can be written as

$$\lambda_{\pm} = e^{\pm\gamma}, \quad (2.97)$$

where γ is the ‘stability exponent’. The eigenvectors

$$\mathbf{L} \boldsymbol{\xi}_{\pm} = \lambda_{\pm} \boldsymbol{\xi}_{\pm} \quad (2.98)$$

describe the unstable ($\boldsymbol{\xi}_+$) and stable ($\boldsymbol{\xi}_-$) directions of the fixed point. Iterating a point which is initially on the ray in the unstable direction, the iterates stay on this line, moving outward according to

$$\boldsymbol{\xi}_n = \mathbf{L}^n \boldsymbol{\xi}_0 = e^{n\gamma} \boldsymbol{\xi}_0. \quad (2.99)$$

Iterates started in the stable direction finally converge to the fixed point. All other points move on a branch of a hyperbola with asymptotes given by the unstable and stable directions, as shown below, iterating finally to infinity in the unstable direction, as illustrated in Fig. 2.17. Such an unstable fixed point is therefore called a ‘*hyperbolic fixed point*’.

For the case $\text{Tr } \mathbf{L} < -2$, the eigenvalues can be written as $\lambda_{\pm} = -e^{\mp\gamma}$, and the behavior is very similar except that the iterates alternate between both branches of the hyperbola. This is a ‘*hyperbolic fixed point with reflection*’.

(b) $|\text{Tr } \mathbf{L}| < 2$: The eigenvalues are complex conjugate and of unit absolute value. They are conveniently expressed as

$$\lambda_{\pm} = e^{\pm i\beta}, \quad (2.100)$$

where β is called the ‘*stability angle*’. In terms of the complex eigenvectors $\boldsymbol{\xi}_{\pm}$, any initial vector

$$\xi_0 = a_+ \xi_+ + a_- \xi_- \quad (2.101)$$

is mapped to

$$\xi_n = \mathbf{L}^n \xi_0 = a_+ e^{+in\beta} \xi_+ + a_- e^{-in\beta} \xi_- . \quad (2.102)$$

These iterates are all restricted to an ellipse, which is rotated in the (x, y) -plane (see below) and the fixed point is called an '*elliptic fixed point*', as illustrated in Fig. 2.18. The fixed point is stable, and any point close to it stays in its neighborhood.

It remains to show that the iterates of the map (2.90) with $\det \mathbf{L} = 1$ trace out a conic section. This can easily be seen by first observing that \mathbf{L} is symplectic, i.e., it satisfies the relation

$$\mathbf{L}^t \mathbf{J} \mathbf{L} = \mathbf{J} \quad (2.103)$$

with

$$\mathbf{J} = \begin{pmatrix} 0 & -1 \\ 1 & 0 \end{pmatrix} . \quad (2.104)$$

Secondly, the set

$$\Sigma_Q = \{ \xi \mid \xi^t \mathbf{J} \mathbf{L} \xi = Q \in \mathbb{R} \} \quad (2.105)$$

is invariant under the map \mathbf{L} . To show this, we take $\xi \in \Sigma_Q$ with image $\xi' = \mathbf{L}\xi$. We then have

$$\xi'^t \mathbf{J} \mathbf{L} \xi' = \xi^t \mathbf{L}^t \mathbf{J} \mathbf{L} \mathbf{L} \xi = \xi^t \mathbf{J} \mathbf{L} \xi = Q , \quad (2.106)$$

which shows that $\xi' \in \Sigma_Q$. Finally, the set Σ_Q is a quadratic form in the variables x and y :

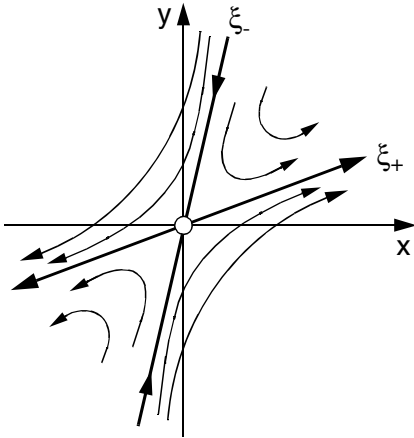


Fig. 2.17. Mapping properties of a hyperbolic fixed point of a two-dimensional linear area-preserving map.

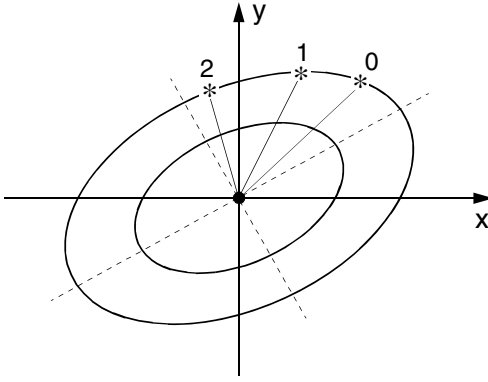


Fig. 2.18. Mapping properties of an elliptic fixed point of a two-dimensional linear area-preserving map.

$$\begin{aligned}
 Q &= \boldsymbol{\xi}^t \mathbf{J} \mathbf{L} \boldsymbol{\xi} = (x, y) \begin{pmatrix} 0 & -1 \\ 1 & 0 \end{pmatrix} \begin{pmatrix} L_{11} & L_{12} \\ L_{21} & L_{22} \end{pmatrix} \begin{pmatrix} x \\ y \end{pmatrix} \\
 &= L_{12} y^2 + (L_{11} - L_{22}) xy - L_{21} x^2.
 \end{aligned} \tag{2.107}$$

This determines a conic section. The reader can easily show that a rotation

$$\mathbf{D}(\chi) = \begin{pmatrix} \cos \chi & -\sin \chi \\ \sin \chi & \cos \chi \end{pmatrix} \tag{2.108}$$

with

$$\tan 2\chi = \frac{L_{22} - L_{11}}{L_{12} + L_{21}} \tag{2.109}$$

and $\mathbf{L}' = \mathbf{D}^t \mathbf{L} \mathbf{D}$ brings the conic section to the standard form

$$Q = L'_{12} y'^2 - L'_{21} x'^2. \tag{2.110}$$

Furthermore, we have

$$L'_{12} - L'_{21} = L_{12} - L_{21} \quad \text{and} \quad L'_{12} L'_{21} = (\text{Tr } \mathbf{L}/2)^2 - 1 \tag{2.111}$$

and one can again verify that an ellipse is obtained for $|\text{Tr } \mathbf{L}| < 2$ and a hyperbola for $|\text{Tr } \mathbf{L}| > 2$.

It is sometimes more convenient to characterize the fixed point by the quantity

$$R = (2 - \text{Tr } \mathbf{L})/4, \tag{2.112}$$

the so-called ‘*residue*’ of the fixed point. The orbit is stable for $0 < R < 1$ with the exception of the values $R = 3/4$ and $R = 1/2$. In the case of stability, the points move on ellipses at a rate ν (rotations per period) with

$$R = \sin^2(\beta/2) = \sin^2(\pi\nu). \tag{2.113}$$

For $R > 1$ or $R < 0$, the orbit is unstable (hyperbolic or hyperbolic with reflection, respectively).

In the cases $R = 0, 1, 3/4, 1/2$, where the eigenvalues are low order roots of unity ($\lambda^k = 1$ with $k = 1, 2, 3, 4$), the linearized map is not sufficient to determine the stability of the fixed point (see [20]).

When a parameter of the (area-preserving) map is varied, the periodic orbits, i.e., the fixed points of the map (2.86) or its iterates, may bifurcate whenever the residue passes a value

$$R_{l,m} = \sin^2(\pi l/m). \quad (2.114)$$

A more detailed discussion of the bifurcation properties of area-preserving maps can be found in the article by Green et al. [21].

2.4.6 Bifurcations

In many situations the structural properties of the dynamics are preserved when parameters of the system are (slowly) varied. There are, however, important exceptions: a bifurcation describes a rapid change in the type of dynamics when parameters of the system cross a critical value. Here, we discuss some important examples.

Pitchfork Bifurcation: Pitchfork bifurcation has been discussed above in the context of one-dimensional maps $x' = f(x, r)$. Let us recall its basic properties: a period-one fixed point of the map becomes unstable when the slope of the derivative $|f'(x, r)|$ passes through unity. At the same time, a pair of stable fixed points of period two appears, as illustrated in Figs. 2.13 and 2.14 above.

Tangent Bifurcation. In a tangent bifurcation a stable and an unstable fixed point approach each other and disappear into the complex plane. In the vicinity of the bifurcation point the system still feels the influence of the previous fixed points; they appear as ‘ghosts’, attracting the orbits for a while until they are ejected again. This leads to so-called ‘*intermittency*’, where an irregular wandering of the orbit is interrupted at irregular intervals by regular dynamics in the vicinity of the (disappeared) fixed points. As an example, such behavior is discussed for one-dimensional maps in Sect. 2.4.4 (compare also the numerical experiments in Chap. 9).

Hopf bifurcation: The Hopf bifurcation describes the transition from a point attractor to a limit cycle [22]. It can be modeled by the differential equations

$$\frac{dr}{dt} = -(g + r^2)r, \quad \frac{d\phi}{dt} = \omega \quad (2.115)$$

in polar coordinates, which can be solved in closed form:

$$r^2(t) = \frac{g r_0^2 e^{-2gt}}{r_0^2 (1 - e^{-2gt}) + g}, \quad \phi(t) = \omega t \quad (2.116)$$

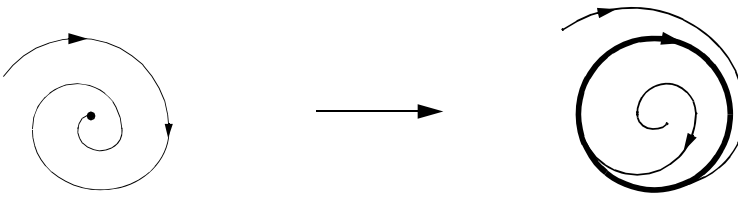


Fig. 2.19. Hopf bifurcation: A point attractor bifurcates into a limit cycle.

with $r(0) = r_0$ and $\phi(0) = 0$. The solution approaches a fixed point at $r = 0$ for $g \geq 0$. When the parameter g is decreased to negative values, a limit cycle of radius $\sqrt{-g}$ appears, which attracts all solutions from inside or outside (see Fig. 2.19).

It is furthermore instructive to linearize the differential equations (2.115) in Cartesian coordinates, yielding

$$\frac{d}{dt} \begin{pmatrix} x \\ y \end{pmatrix} = \begin{pmatrix} -g & -\omega \\ \omega & -g \end{pmatrix} \begin{pmatrix} x \\ y \end{pmatrix}. \quad (2.117)$$

The eigenvalues of the matrix are $\lambda_{\pm} = -g \pm i\omega$. At the bifurcation point $g = 0$, a pair of complex conjugate eigenvalues crosses the imaginary axis, which is characteristic for a Hopf bifurcation. A numerical study of a Hopf bifurcation can be found in the computer experiment in Sect. 12.3.2.

References

1. J. Guckenheimer and P. Holmes, *Nonlinear Oscillations, Dynamical Systems, and Bifurcations of Vector Fields*, Springer, New York, 1983
2. A. J. Lichtenberg and M. A. Lieberman, *Regular and Stochastic Motion*, Springer, New York, 1983
3. J. M. T. Thompson and H. B. Stewart, *Nonlinear Dynamics and Chaos*, John Wiley, Chichester, 1986
4. H. G. Schuster, *Deterministic Chaos*, VCH, Weinheim, 1988
5. M. Ozorio de Almeida, *Hamiltonian Systems – Chaos and Quantization*, Cambridge University Press, Cambridge, 1988
6. M. Tabor, *Chaos and Integrability in Nonlinear Dynamics*, John Wiley, New York, 1989
7. G. L. Baker and J. P. Gollub, *Chaotic Dynamics – An Introduction*, Cambridge Univ. Press, Cambridge, 1990
8. J. Frøyland, *Introduction to Chaos and Coherence*, IOP Publishing, Bristol, 1992
9. Hao Bai-Lin, *Chaos*, World Scientific, Singapore, 1984
10. P. Cvitanović, *Universality in Chaos*, Adam Hilger, Bristol, 1984
11. R. S. MacKay and J. D. Meiss, *Hamiltonian Dynamical Systems*, Adam Hilger, Bristol, 1987
12. D. Ruelle, *Strange attractors*, Math. Intelligencer **2** (1980) 126, reprinted in: P. Cvitanović, *Universality in Chaos*, Adam Hilger, Bristol, 1984

13. S. Smale, *Diffeomorphisms with many periodic points*, in S. S. Cairns, editor, *Differential and Combinatorial Topology*. Princeton University Press, Princeton, 1963
14. D. Ruelle and F. Takens, *On the nature of turbulence*, Commun. Math. Phys. **20** (1971) 167, reprinted in: Hao Bai-Lin, *Chaos*, World Scientific, Singapore, 1984
15. S. E. Newhouse, D. Ruelle, and F. Takens, *Occurrence of strange axiom A attractors near quasiperiodic flows on T^m , $m \geq 3$* , Commun. Math. Phys. **64** (1978) 35
16. P. Manneville and Y. Pomeau, *Intermittency and the Lorenz model*, Phys. Lett. A **75** (1979) 1
17. Y. Pomeau and P. Manneville, *Intermittent transition to turbulence in dissipative dynamical systems*, Commun. Math. Phys. **74** (1980) 189, reprinted in: Hao Bai-Lin, *Chaos*, World Scientific, Singapore, 1984 and P. Cvitanović, *Universality in Chaos*, Adam Hilger, Bristol, 1984
18. G. D. Birkhoff, *Nouvelles recherches sur les systèmes dynamiques*, Mem. Pont. Acad. Sci. Novi Lyncaei **1** (1935) 85
19. M. V. Berry, *Regular and irregular motion*, in S. Jorna, editor, *Topics in Nonlinear Dynamics*, page 16. Am. Inst. Phys. Conf. Proc. Vol. 46, 1978. Reprinted in R. S. MacKay and J. D. Meiss, *Hamiltonian Dynamical Systems*, Adam Hilger, Bristol, 1987
20. K. R. Meyer, *Generic Bifurcations of Periodic Points*, Trans. AMS **149** (1970) 95
21. J. M. Greene, R. S. MacKay, F. Vivaldi, and M. J. Feigenbaum, *Universal behaviour in families of area-preserving maps*, Physica D **3** (1981) 468, reprinted in: R. S. MacKay and J. D. Meiss, *Hamiltonian Dynamical Systems*, Adam Hilger, Bristol, 1987
22. J. E. Marsden and M. McCracken, *The Hopf Bifurcation and Its Applications*, Springer, New York, 1976

Chaos

A Program Collection for the PC

Korsch, H.J.; Jodl, H.-J.; Hartmann, T.

2008, XV, 341 p. With many Numerical Experiments.,

Hardcover

ISBN: 978-3-540-74866-3